Journal Name

ARTICLE TYPE

Cite this: DOI: 00.0000/xxxxxxxxxx

Computational study of the staircase molecular conductivity of polyoxovanadates adsorbed on Au(111)†

Almudena Notario-Estévez,[a] Xavier López,*[a] and Coen de Graaf*[a,b]

Received Date
Accepted Date

DOI: 00.0000/xxxxxxxxxx

This computational study presents the molecular conduction properties of two members of the polyoxovanadate (POV) class of molecules, V_6O_{19} (Lindqvist-type) and $V_{18}O_{42}$, which have been targeted as possible successors of the materials that are currently used in complementary metal-oxide semiconductor (CMOS) technology. Molecular conductivity calculations on the Lindqvist-type POV absorbed on Au(111) shows a staircase conductivity as function of the applied bias voltage, which is directly related to the oxidation state of the absorbed molecule. After these proof-of-principle calculations we applied the same technique to the larger $V_{18}O_{42}$, a system featuring many more easily attainable redox states, and hence, in principle even more interesting from the multiple-state resistive (memristive) viewpoint. The calculated transmission strongly suggests that this molecule does not possess staircase conductivity, a fact ascribed to the large number of unpaired electrons in the resting state.

1 Introduction

Polyoxovanadates (POVs) constitute a sub-class of the vast polyoxometalate (POM) family[1–6] with outstanding physicochemical properties and potential applications.[7–9] The majority of POM compounds present highly symmetric shapes, and are made of oxygen and early transition metals in their highest oxidation states, typically W^{VI} and Mo^{VI}, less commonly Nb^{V}, V^{V} and others.[10] Despite being anionic compounds, the formally high oxidation states of the metal centres allow fairly easy molecular reduction in general, altering their behaviour while keeping the structural integrity. This redox lability is a fingerprint of POMs. Yet, some characteristics of POVs differentiate them of their parent family, increasing their potential impact as central motifs in high added-value applications, notably in magnetism[11–14] and catalysis.[15,16] Two main reasons make POVs especially attractive: i) they benefit from a larger variety of truly accessible oxidation states for vanadium (2+ to 5+), a plus in many fields of Chemistry. As a matter of fact, POVs with non-classical architectures are, by definition, prone to mixed-valency in their metal centres; ii) their molecular topology; the distinctive pseudo-spherical shapes and large range of nuclearities confer these systems a great potential for application in devices designed at the molecular scale. As an additional important feature, experiments have shown that some POVs present variable electrical conductance depending on their redox state. Because these are relatively easy to access upon minor external stimuli,[17] they are candidates for acting in resistive switching cells. In a practical approach, control at the molecular scale is crucial to make the resistive memory-based computer technology a reality,[18,19] bypassing some technical difficulties such as electron tunnelling effects known in nowadays' microelectronics. In addition, implementation of discrete energy levels typical of POMs, instead of the band structure of a dielectric solid-state material, is another advantage. These points are beneficial if the memristive functionality[20,21] operates with multiple resistive states (MRS) that appear from changes in the many stable, metal-centred redox states. In this field of application, POVs present a unique interplay between the molecular charge, the redox properties (mostly associated with $V^{IV/V}$) and the spin degrees of freedom.[22–24] Development of physical and chemical approaches to obtain and operate these systems at the molecular level can help materialize this technology and the access to new functionalities.

The present study extends the theoretical research in the POV field started in our group some years ago.[25–29] Some of these articles describe the electronic structure and the complex magnetism of the $V_{18}O_{42}$ and $V_{22}O_{54}$ members of the family. In other works we thoroughly explored the solution behaviour of $V_{18}O_{42}$ to understand the impact of the solvent, the countercations and the POV redox state on the formation of ion pairs and the phenomenon of molecular agglomeration. In all these studies, the in-

[a] Universitat Rovira i Virgili, Departament de Química Física i Inorgànica, Marcel·lí Domingo 1, 43007 Tarragona, Spain; E-mail: javier.lopez@urv.cat, coen.degraaf@urv.cat
[b] ICREA, Pg. Lluís Companys 23, Barcelona 08010, Spain.

† Electronic Supplementary Information (ESI) available: [Figures: Adsorption modes and orientations of V6 on Au(111); Projected density of states of isolated and adsorbed V6-S-CH3 and V6-S-Ph on Au(111); Projected density of states of V6-S-Ph adsorbed on Au(111); Projected density of states of V18 (10:8) in isolated and adsorbed forms with two different adsorption modes; Plots of transmitting eigenchannel scattering states of V18 in three redox forms. Tables: Relative interaction energies and distances of V6 on Au(111) in different modes; Bader charges per fragment for V18–Au (8:10, 10:8 and 12:6 states)]. See DOI: 00.0000/00000000.

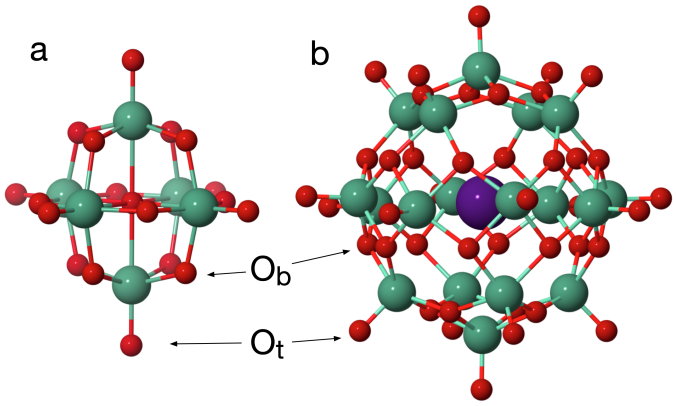

Fig. 1 Ball-and-stick representation of a) $[V_6O_{19}]^{2-}$ and b) $[I@V_{18}O_{42}]^{5-}$ structures, with oxygen and vanadium atoms in red and green, respectively. The larger purple sphere in b corresponds to the internal I^-. In either structure, terminal (O_t) and bridging (O_b) oxygens are observed.

terplay between experiment and theory was crucial to unravel the physicochemical intricacies of such compounds. Quite recently, we have undertaken the computational study of a functionalized POV structure with the classical Lindqvist architecture, V_6O_{19}, adsorbed on metal surfaces[30] to extract information about the absorption properties in a device-like setup, such as the one adopted in nanoelectronics. The latter project has been motivated by the progress made by Dr. Monakhov and co-workers on the deposition and characterization of POV molecules on gold surfaces in the search for applications.

The present computational work goes one step further and focuses on the molecular conductivity of POVs, similar to a recent work by Georgiev and co-workers on a single-molecule junction with the $W_{18}O_{54}(SO_3)_2$ POM system.[31] Our study is based on periodic density functional theory (DFT) calculations and compares the characteristics and behaviour of two POV systems based on the V_6O_{19} and $V_{18}O_{42}$ architectures[9,32] (V6 and V18 for short, represented in Figure 1). We present the results obtained in adsorbed form on gold and in isolated form to probe how adsorption affects these POVs in terms of stability, electronic structure, but most of all, the conductivity. Besides the evident difference in size between V6 and V18, it is worth stressing that they also differ intrinsically in the fact that V6 has all-V^V centres by nature, whereas V18 presents a mixture of V^V and V^{IV} in the resting state. Note that the V^V and V^{IV} notation is a purely formal one as most of the V atoms in V18 have a mixed-valence character, with an effective oxidation state somewhere between IV and V.[29] This results in dissimilar available molecular redox states, a fact that may have an impact on the response of the gold-POV devices to external electrical stimuli. The calculations presented in the remainder of the paper show that the staircase conductivity in V6 is directly correlated with the redox state of the POV and that such behaviour is not expected for the larger V18 system. We will discuss strategies to design device setups in which a larger number of easily accessible redox states is combined with staircase conductivity.

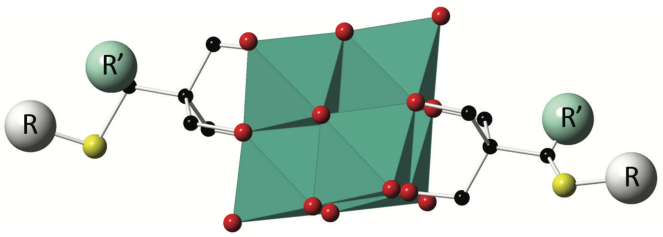

Fig. 2 Schematic representation of the different Lindqvist-type hexavanadate molecules used in the experiment[30] and as template for the models in the present computational study. Red: oxygen, black: carbon, yellow: sulphur. One vanadium atoms is located in the center of each green octahedron, and hydrogens are omitted for clarity. R and R' are small organic substituents.

2 Computational details

2.1 Polyoxovandate molecules

The bare Lindqvist-type hexavanadate V6 presents a 8- charge and a very high q/m ratio of 1.33, which makes this system not workable in any experimental setup. The q/m parameter[33] represents in a simple manner the molecular charge density combining the molecular charge and the number of metal centres in a POM and, thus, it accounts for the intrinsic instability of the system. Therefore, the V6 needs to be functionalized with side groups that lower the total charge without significantly influencing the geometry of the core structure, or its electronic structure. On the other hand, q/m = 0.28 for $[I@V_{18}O_{42}]^{5-}$ and, therefore, there is no need for stabilizing ligands in V18. We have studied the properties of the resting state, plus the oxidized and reduced forms, $[I@V_{18}O_{42}]^{q-}$, that is q = 5, 3 and 7, respectively. The three species are referred to hereafter as V18(10:8), V18(12:6) and V(8:10), where the numbers in parentheses denote the formal number of V^{IV} and V^V centers, respectively.Figure 2 shows the structure used in the experiments: the basic V_6O_{19} structure is decorated with two pentaerythrithol-based ligands extended with –S-R and -R' substituents. Among the different systems that were studied experimentally, we have selected the ones with R' = H, and R = CH_3 (V6-S-Me) or phenyl (V6-S-Ph) to investigate the adsorption properties. In the study of the molecular conductivity we have compared the electronic structure of V6-S-Ph to a simpler model (V6) in which R' = H and the S-R group is replaced with a hydrogen atom.

2.2 Adsorption on Au

The material model consists of a unit cell containing a slab of five 10×8 layers of gold atoms representing an infinite Au(111) surface, the vanadium POM adsorbate and potassium counterions to ensure charge neutrality of the system. Density Functional Theory (DFT) calculations were performed with the Vienna Ab initio Simulation Package (VASP 5.3.5).[34–37] On the basis of previous studies of closely related systems,[38–40] we applied the generalized gradient approximation-type (GGA) exchange-correlation functional by Perdew and Wang (PW91),[41] which suffices to describe not too strong electron correlations, such as found in fully oxidized POMs. A plane wave basis set was used with a 500 eV ki-

netic energy cutoff. For the 1e-, 2e- or 3e-reduced V6 system, the assumed delocalized nature of the extra electrons at room temperature ensures that each vanadium holds an average of 1/6, 1/3 or 1/2 electrons in the 3d-shell, respectively. This average number of electrons per metal center is sufficiently low to avoid strong electron correlations, hence there is no need to apply a GGA+U scheme. We considered the following atomic valence electrons: Au: $5d^{10}6s^1$, C: $2s^2 2p^2$, H: $1s^1$, O: $2s^2 2p^4$, S: $3s^2 3p^4$, V: $3d^3 4s^2$ and K: $3s^2 3p^6 4s^1$, where the core electrons were represented by the Projector Augmented Wave (PAW) method.[42,43] This computational setup results in a lattice parameter for the gold bulk of 4.17 Å, which is in reasonable agreement with the experimental value (4.07 Å).[44,45] Accordingly, the dimensions of the unit cell are $a = 29.52$ Å and $b = 23.62$ Å (where $\alpha = \beta = 90^\circ$ and $\gamma = 120^\circ$). The length along the c direction was set to 30 Å including a vacuum region of ≈17 Å, which was proven to be sufficient to avoid interactions between cell replicas. The isolated molecules were calculated with the same box without the surface.

Solvent effects were not considered, since the experimental measurements were performed after removing the solvent that was used to deposit the POV complexes on the gold surface. To ensure charge neutrality in the unit cell, we added some K^+ counterions to the unit cell. Although it is difficult to ascertain the exact position of these counterions, the opposite charges of counterions and POV suggest that these species stay close to each other when the solvent is removed in the experimental setup.

We modeled a low-coverage regime for the POM-Au system with non-interacting adsorbed molecules (POM–POM distance > 7.5 Å). The POM–Au models were relaxed fixing the three bottom layers of the slab to the geometry obtained in the bulk calculation. The optimizations were performed until self-consistency with thresholds of 10^{-5} eV and 0.02 eV·A^{-1} for electronic and ionic convergence, respectively. The Brillouin zone was sampled with the Monkhorst-Pack grid.[46,47] A 9×9×9 mesh of k-points was applied to run geometry optimizations of the bulk, and for the surface optimizations we used a 7×7×1 mesh. Nevertheless, only the Γ-point was taken into account for the optimization of the POM–Au system due to the large size of the unit cell used. Discussion of atomic charges and spins is based on Bader's AIM (Atoms in Molecules) method[48] using the Henkelmann algorithm for the integration over the atomic basins.[49]

The external homogeneous electrostatic field was defined through a dipole operator, activating the appropriate dipole corrections to the potential to avoid interactions between neighboring images.

2.3 Molecular conductivity

Transport calculations were performed on the optimized POM-Au systems, using version 4.1 of the SIESTA/TRANSIESTA code and the post-processing TBtrans package.[50,51] PW91 was used as exchange-correlation functional.[41] For all the atoms, except for gold, the valence electrons were described using a double-zeta basis set and the core electrons by norm-conserving Troullier-Martin pseudopotentials.[52,53] For gold atoms, a single-zeta basis set was used in combination with a pseudopotential which accounts only for 1 valence electron. This apparently crude description gives reasonably good transport properties in single-point calculations.[54,55] We gradually increased the number of k-points until convergence of the DOS, first for the gold electrodes and, second, until convergence of the transmission function of the device. These calculations gave us a grid of 13×13×7 for the TRANSIESTA calculations and 27×27×21 for TBtrans. For electron-reduced systems, only the countercations were optimized in the complete POM-Au(111) system, keeping the POM-Au(111) structure of the completely oxidized system.

3 Results and discussion

In the following, we discuss the outcomes of the calculations performed on the two above-mentioned V6 derivatives. First, their adsorption properties are summarized and, then, we show that V6 shows staircase molecular conductivity because of the changes in the oxidation state as function of the applied voltage. Next we follow the same procedure for V18.

3.1 Adsorption properties of V6 on Au(111)

DFT geometry optimizations were performed for V6-S-Me and V6-S-Ph on the Au(111) surface. There are two different adsorption modes; the octahedral molecule can either make contact with the gold surface through one of the faces or one of its edges. The presence of the stabilizing ligands limits the possibilities to just one face and one edge as shown in Fig. 3. The edge orientation has three direct oxygen-gold contacts, while the face orientation presents six contacts. In addition, there are four different adsorption sites on the surface: top, hcp, fcc and bridge, as shown in Fig. 4, taking the central oxygen atom of V6 as reference for identifying the different adsorption sites. Finally, there is one more degree of freedom for the adsorption related to the orientation of V6, which can be aligned to two different lattice vectors as indicated in Fig. 4. For the face orientation, these possibilities have been studied before for the related Mo_6O_{19} Lindqvist POM on Au(111).[56] Following the conclusions of that study, we have only considered the fcc adsorption site here. Less is known about the edge orientation and, therefore, we have tested the four positions and the two different directions on the gold surface.

Geometry optimizations of the fully oxidized forms of V6-S-Me and V6-S-Ph, with net charge 2-, lead to slightly negative bonding energies of the order of -0.6 eV. Although this energy is not very large and actually at the border of physisorption and chemisorption, we will refer to it as adsorption for simplicity. The relative interaction energies for the different modes analyzed do not differ by more than 0.34 eV. In both derivatives, the face(fcc) and edge(t_1) are the most stable structures. Because of the presence of phenyl groups that are prone to strong dispersion interactions with the metal surface, we have repeated the face(fcc) and edge(t_1) calculation for V6-S-Ph taking into account explicitly the dispersion with Grimme's D2 correction.[57] This interaction drags the phenyl rings towards the Au surface, which is most noticeable for the edge(t_1) structure, since one of the phenyl rings in the face(fcc) structure is already close to the surface without the dispersion correction. Hence, the edge(t_1) is now slightly more

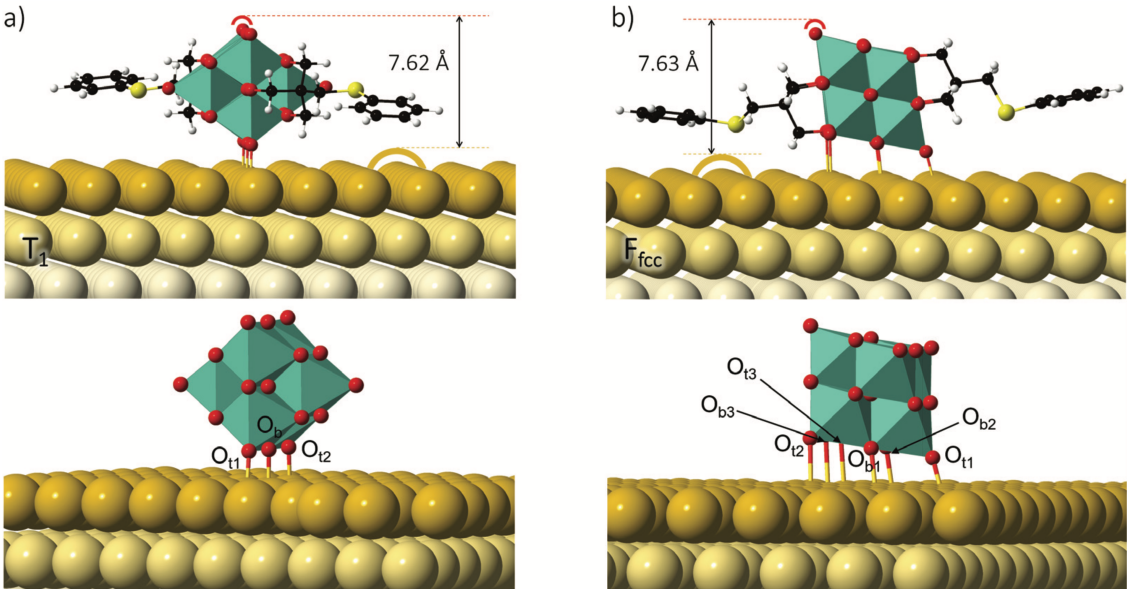

Fig. 3 Upper part: Optimized geometries of V6-S-Ph on Au(111) in the T1 adsorption side (a) and fcc site (b). Lower part: labels of the oxygen atoms exposed to the surface in the edge (a, three contacts) and the face (b, six contacts) adsorption modes. Ligands are omitted for clarity in the lower panel.

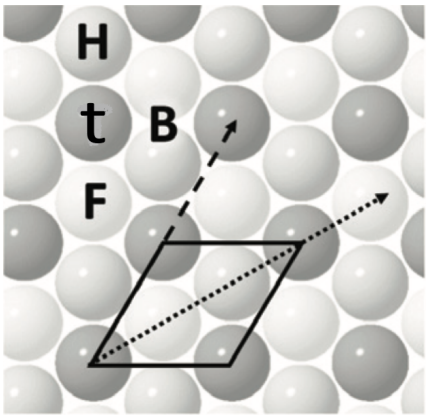

Fig. 4 hcp (H), top (t), fcc (F) and bridge (B) adsorption sites of the Au(111) surface. The gold atoms in the different layers are represented with different gray scales, the darkest belonging to the top layer. The two possible orientations of the adsorbed species are indicated by the dashed (1) and dotted (2) vectors.

favorable by 0.12 eV compared to the face(fcc). This difference is however not large enough to identify this structure as the only possible adsorption mode; it is most likely that both face and edge adsorption modes at different sites are possible, leading to a somewhat disordered disposition of the V6 molecules on the surface.

The face(fcc) and edge(t_1) geometries of V6-S-Ph have the top of the adsorbed POV 7.62 and 7.63 Å above the gold surface, respectively, in good agreement with the experimental estimate of 7.5 $\pm$ 0.05 Å. These values take into account the van der Waals atomic radii of 1.52 for O and 1.66 Å for Au atoms (see Figure 3).[58,59] For V6-S-Me, the computed heights are 7.66 Å (edge(t_1)) and 7.63 Å (face(fcc)). The dispersion effects decreases the height by about 0.40 Å for edge(t_1), and only 0.17 Å for face(fcc), in line with the observation made before that the latter structure already has one phenyl group on the surface without dispersion. The O-Au contacts involve both bridge and terminal oxygens (O_b and O_t). Edge(t_1) adsorption presents three O-Au contacts, one of them of O_b type and two O_t. On the other hand, face(fcc) presents six contacts, three O_b and three O_t. The O-Au distances in the edge(t_1) mode range within 2.32-2.40 Å for V6-S-Me and 2.31-2.37 Å for V6-S-Ph. For face(fcc) the oxygen-Au distances fall in the 2.34-3.25 Å interval for both compounds. Pictures of the adsorption geometries, the relative interaction energies and the O-Au distances can be found in Figure S1 and Table S1 in the supplementary information.

Having identified the face(fcc) and edge(t_1) as the most stable adsorption geometries for both V6-S-Me and V6-S-Ph, we analyze the effect of the interaction with the gold surface on the electronic structure of the adsorbate. For that goal, the density of states (DOS) and the Bader charges of the adsorbed and isolated molecules are compared. As already shortly discussed in Ref. 30, the DOS of the adsorbed species are very similar to those calculated in their isolated forms, especially the projected DOS of the occupied oxygen and empty V-3d levels, i.e., the V_6O_{19} core structure of the adsorbed molecules (see Figure S2 in the supplementary information). The only apparent difference appears for the C/S levels in the t_1 adsorbed molecules, which were found close to the V-3d band, while they are separated by $\sim$0.5 eV in all other cases. This relative high energy can be ascribed to the weak contact between ligands and the gold surface in this orientation compared with the face(fcc) mode.

A second indication that the molecules remain chemically intact upon adsorption, and that they are not oxidized or reduced by the surface, is provided by the Bader atomic charges calculated for the system. The atomic charges listed in Table 1 indicate a net charge of $\sim$1.9- for the adsorbed molecules, virtually the same as

	site	Σ V6-atoms	Σ counterions	Σ Au atoms
V6-S-Me	edge(t_1)	-1.92	1.83	0.09
	face(fcc)	-1.90	1.83	0.07
V6-S-Ph	edge(t_1)	-1.90	1.83	0.07
	face(fcc)	-1.93	1.83	0.10

Table 1 Bader atomic charges computed for the Lindqvist-type derivatives adsorbed on gold in two different modes

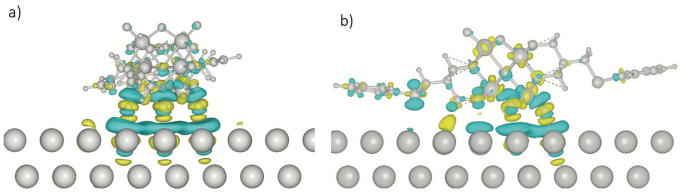

Fig. 5 Charge difference $\Delta\rho$ for the adsorption of V6-S-Ph in (a) face(fcc) and (b) edge(t_1). Yellow and blue regions represent accumulation and depletion of the electron density, respectively. The surface isovalue is set to 0.001 e/Bohr^3

Atom	E_{ext}	1e$^-$-reduced	2e$^-$-reduced	3e$^-$-reduced
V1	0.12	0.08	0.31	0.30
V2	0.23	0.25	0.31	0.31
V3	0.09	0.06	0.38	0.54
V4	0.26	0.37	0.38	0.40
V5	0.13	0.10	0.28	0.43
V6	0.25	0.23	0.29	0.45

Table 2 Mulliken atomic spin populations for the vanadium atoms in V6-S-Ph adsorbed in face(fcc) mode for the fully oxidized form under the influence of an external electric field and for the 1, 2 and 3-electron reduced forms

the net charge of 2- in isolated form.

To gain additional insight into the nature of the adsorption we have considered the gold surface and the V6 adsorbate as two interacting fragments. In isolated form, their corresponding electron density distribution functions are ρ(Au) and ρ(V6). When both fragments are put together at the adsorption geometry, these ρ evolve to ρ(Au + V6), which is not equal to the sum of the initial densities. The charge density difference ($\Delta\rho$) refers to the change experienced by the total electron density distribution of surface and adsorbate upon mutual interaction: $\Delta\rho = \rho(\mathrm{Au+V6}) - \{\rho(\mathrm{Au}) + \rho(\mathrm{V6})\}$. At variance with ρ, $\Delta\rho$ can take positive (accumulation of ρ) or negative (depletion of ρ) values at any point in space. The most intuitive way of interpreting $\Delta\rho$ is to represent a surface connecting points of the same value and sign, thus identifying regions of accumulation or depletion of ρ. Fig. 5 represents such isovalue surface for V6-S-Ph in the two adsorption modes studied. A region of electron density depletion ($\Delta\rho < 0$, blue colour) is located in between the two fragments, indicative of a non-covalent interaction. This feature, distinctive of weakly or moderately interacting fragments, denotes minor changes in the electronic structure and implies that the chemical integrity of the fragments is mostly maintained. A second conclusion that can be drawn from this figure is that the sulphur atoms and the phenyl ring only play a minor role in the adsorption process. As a consequence of their relatively large distance from the surface, the changes in the electron density in the S-Me or S-Ph regions are minimal. It is safe to say that the V6 molecules connect to the surface via the Au-O contacts depicted in Fig. 4.

3.2 Application of an external electric field

To answer the question whether an external potential can reduce the adsorbed species, we have introduced an external electric field (E_{ext})in our computational setup. The effect of applying E_{ext} = 0.5 eV· Å^{-1} has been analysed for the two model compounds. The Bader analysis evidences that the adsorbed molecules are reduced under such an electrical field, with a calculated molecular charge increase of almost one unit, up to –2.72 for V6-S-Ph in face(fcc). Concomitantly, the gold slab is oxidised by 0.90 electrons. In line with these results, the energy of the lowest vanadium d-band is downshifted by the effect of the electric field, fully hitting the Fermi level now and accepting electron density from gold. Moreover, the Mulliken atomic spin populations (MASP) (column 2, Table 2) indicate that the extra electron is shared by the six V atoms of the adsorbed molecule.

To complete the picture, we have studied the one-, two- and three-electron reduced adsorbed molecules (without external electric field). Upon one-electron reduction, the α-PDOS reveals that the vanadium d-band crosses the Fermi level and becomes partially filled as observed when an electric field was applied on the fully oxidized form. The β-PDOS does not suffer significant changes. The filling of the vanadium d-levels is corroborated by the Mulliken atomic spin densities (see Table 2). For the 2e-reduced compound we considered the lowest triplet state, although the ground state is actually a singlet by virtue of the well-known strong antiferromagnetic coupling occurring in 2e-reduced POMs.[60] The coupling of the unpaired electrons is actually so strong that these 2e-reduced POMs behave as diamagnetic species.[61,62] Both solutions have, though, very similar electronic spatial distributions[63] and, to simplify the electron count of the delocalized d-electrons, Table 2 lists the MASPs taken from the triplet calculation. Confirming that both solutions are practically identical, the total charge of the singlet closed-shell for the POM has been computed to be close to the one found in the high-spin solution. Successive reductions associated to an applied electric field involve a steady filling of the vanadium d-band in the V_6O_{19} unit and a concomitant increase in the MASP of V atoms.

3.3 Molecular conductivity in V6

The second part of the study focuses on the molecular conductivity of the V6-Au system. Attention is centered on two questions: (i) can the different plateaus observed in the $I-V$ plots be ascribed to successive oxidation states of the adsorbed molecules? and (ii) are the conductivity channels through the molecule dominated by contributions from the V-atoms? We have calculated the conductivity of four different systems: the completely oxidized and the one-, two- and three-electron reduced systems. These results allow us comparing the electrical conduction as a function of the oxidation state of the system with the experimental $I-V$

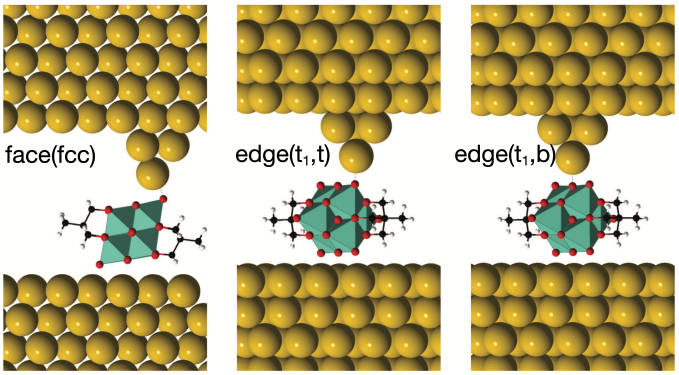

Fig. 6 Device geometries in the molecular conductivity of V6 on Au(111)

data.

3.3.1 Device model

Compared to the previously described adsorption study, molecular conductivity calculations are much more expensive. First, a second slab of gold atoms with a model tip has to be introduced, and second, the computational approach to calculate the conductivity relies on non-equilibrium Green's functions whose handling is significantly more complex than the plane wave basis used so far. Therefore, we have first reconsidered the necessity of explicitly including the ligands in the device model. The first observation that we have used is the experimental similarity of the $I-V$ plots for V6-S-Me and V6-S-Ph. Combined with the nearly indistinguishable DOS of the molecules adsorbed on Au(111), V6-S-Ph was discarded for the conductivity calculations. This reduces significantly the minimal size of the unit cell to avoid interactions between images of the molecule in neighboring cells. Next, we take into account that the role of the sulphur atoms in the adsorption is small, which allows us to replace the S-Me group with a hydrogen, leaving the Lindqvist V6 molecule only capped with two pentaerythrithol ligands. As shown in Figure S3 in the supplementary information, this replacement has negligible effects on the DOS. A further reduction of the model by removing the pentaerythrithol ligands and saturate the bonds with hydrogens (Model 2) leads to small but noticeable changes in the DOS and was not further considered. The pentaerythrithol-capped V6 unit is placed between two Au(111) surface of which the upper one is extended with a minimal tip model consisting of four gold atoms in a tetrahedral arrangement. Figure 6 shows the three device geometries that were finally considered. One with the V6 in face(fcc) adsorption and the tip connecting to the terminal oxygen that is sticking out most, and two in edge(t_1) adsorption. The last two make contact with the tip through a terminal or a bridging oxygen.

3.3.2 Transmission spectra and $I-V$ curves

The zero-bias transmission spectra calculated for the fully oxidized V6 in these three set-ups are shown in Fig. 7. The comparison shows that the position of the tip has a significant influence on the position and intensity of the transmission peaks. An intense peak appears near the Fermi level when the tip connects with the terminal oxygen of the V6. This peak has practically zero intensity when there is a tip-V6 contact through a bridging oxygen. Furthermore, it is clear that the adsorption mode is relatively unimportant; the face(fcc) and edge(t_1,t) spectra are similar in the region close to the Fermi level.

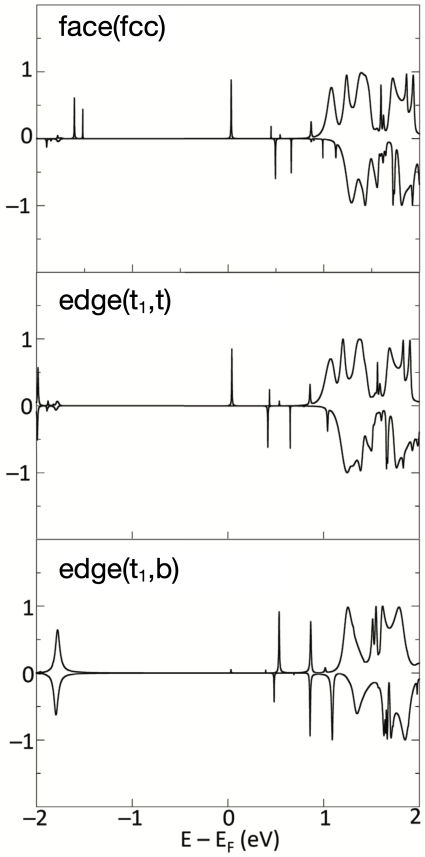

Fig. 7 Calculated transmission spectra of the three device set-ups at zero bias potential.

Transmission spectra at zero bias are useful to get an idea of the current that may flow through the molecule when a bias potential is applied, but for a more quantitative analysis, one has to calculate these spectra at non-zero bias. The application of a bias voltage moves the transmission peak to higher energy but a part of the peak stays inside the bias window (the shaded areas in Fig. 8), meaning that there is indeed a current flowing through the molecule. The transmission spectra for the face(fcc) species are indistinguishable from the edge(t_1,t) ones, therefore we have performed the study of the transmission for the reduced species only for the latter.

By reducing the V6 on the Au(111) surface, the V-band gains electron population. As these levels are assumed to be the constituents of the conduction channels through the molecule, more peaks are expected in the transmission spectrum close to the Fermi energy. Figure 9 compares the zero-bias transmission spectrum of Fig. 7 to those of the one-, two- and three-electron reduced V6 molecules adsorbed on Au(111). As most salient feature, we remark that the fully oxidized species only has one clear peak close to E_F, and that this number steadily increases upon one- and two-electron reductions (yellow and red curves). The situation for the three-electron case (dark pink) is somewhat more complicated as several low-intensity peaks appear close to

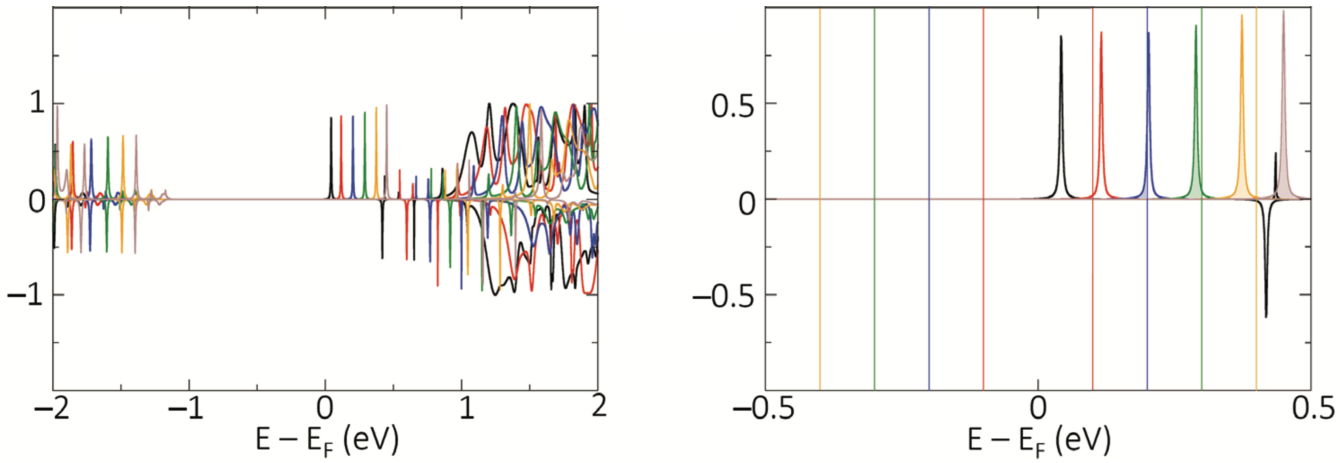

Fig. 8 Transmission spectra of the fully oxidized V6 adsorbed as edge(t_1,t) at different bias voltages: black, red, blue, green, yellow and dark pink correspond to 0, 0.2, 0.4, 0.6, 0.8 and 1 V. The right panel zooms in on the region around the Fermi level, where vertical colored lines mark the bias window and the shaded areas mark the part of the transmission peak that falls inside each window.

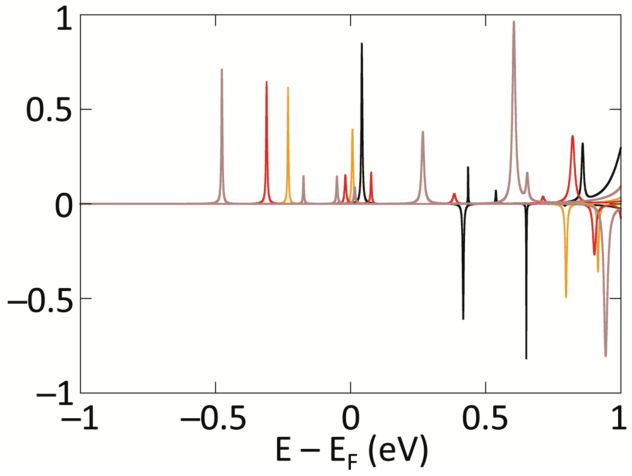

Fig. 9 Zero-bias transmission spectra for the fully oxidized V6 (black) and the one-, two-, and three-electron (yellow, red, dark pink) reduced V6 on Au(111).

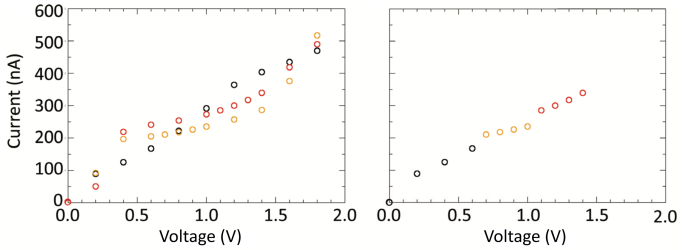

Fig. 10 $I-V$ plot for zero- (black), one- (orange) and two- (red) electron reduced (t_1,t). The staircase trend can be appreciated in the panel on the right, where only the experimentally observed species is plotted at every potential.

E_F.

The increase in the number of transmission channels leads indeed to stronger current when the bias voltage increases. However, the number of peaks inside the window is not the only factor, the intensity of these peaks is as important for the final estimate of the current. As can be seen in the right panel of Fig. 8, the surface of the peak inside the bias window tends to grow for larger bias. This latter effect apparently complicates the interpretation of the current versus voltage for the different redox states of the V6 molecules. The left panel of Fig. 10 shows the current-potential ($I-V$) dependence for the fully oxidized and the reduced forms. At first sight, no clear tendency can be recognized, apart from an overall increase of the current with increasing potential. However, one important factor is not accounted for in this plot, which is that increasing bias voltage leads to reduction. The black points at the higher voltage do not make physical sense, because at these bias potentials the molecule is reduced, probably multiple times.

The relative stability of the different redox states of the V6 on Au(111) is very difficult to assess by computation. This is a general problem for computational chemistry; comparing total energies of systems with a different number of electrons is highly complicated. In the previous section we have seen that the application of an external electric field of 0.5 eV/Å transfers one electron from the surface to the V6 molecule, approximately coinciding with the voltage where a first sudden increase in the conductivity was observed in experiment.[30] Assuming that at each step in the conductivity the system is reduced, the left panel of Fig. 10 can be simplified by removing the points belonging to the (at that voltage) unrealistic redox states. From 0 to 0.65 V, only the current of the fully oxidized form are shown, from 0.66 to 1.06 V we draw those corresponding to the one-electron reduced state and for higher voltages, the points for the two-electron reduced molecule are taken.

The removal of the unrealistic data points uncovers an approximate staircase behaviour in the conductivity and function of the bias voltage, similar to observed in experiment (see also the overlay of the experimental and theoretical data in the supplementary information). This becomes even more clear by comparing the experimental dI/dE and the calculated dI/dV plots in Fig. 11. After the first reduction around 0.6 V, the current stays relatively constant and undergoes a second increase upon a second reduction

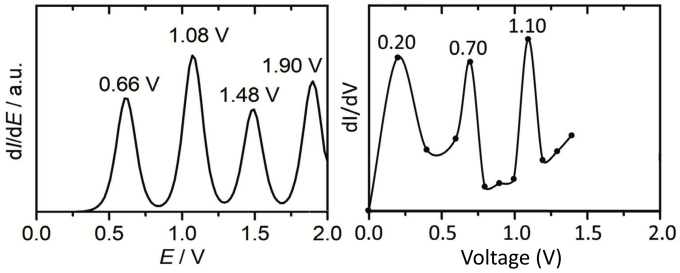

Fig. 11 Experimental (left)[30] and calculated dI/dV plots.

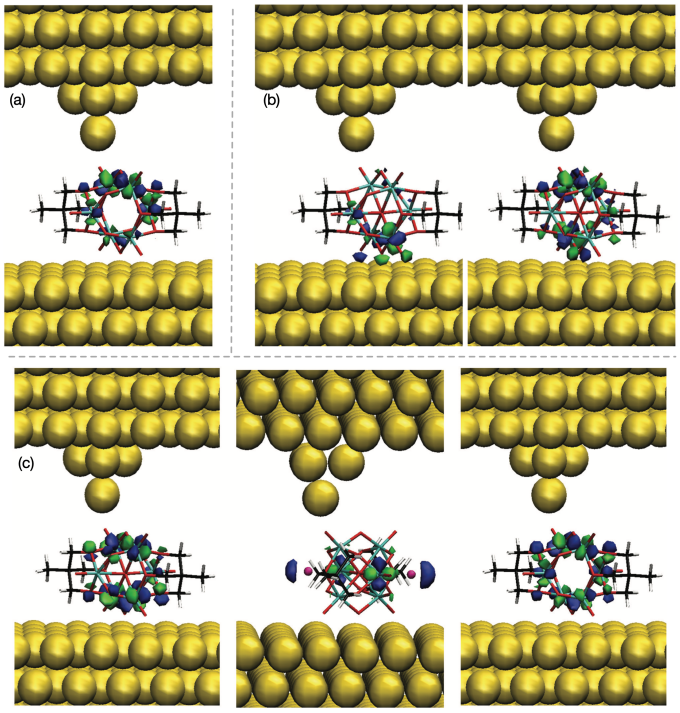

Fig. 12 Most transmitting scattering states for (a) the fully oxidized, (b) one-electron reduced and (c) two-electron reduced capped-V6 on Au(111).

at bias voltage of 1.1 V. The simple two-point estimate for the gradient at each calculated point breaks down for 0.2 V as the current at 0 V is zero by definition. More sophisticated estimates of the gradient with three- or five-point estimates would require much more data points. This is unfortunately not realistic at this point given the large computational cost of these calculations.

The most transmitting eigenchannel scattering states[64,65] of the capped-V6 adsorbed in the edge(t_1,t) position with different oxidation states at E_F are shown in Fig. 12. In all cases the eigenchannels are strongly dominated by the contributions of the V-3d orbitals, which is of course not fully unexpected as the V-3d levels are the ones that are closest to the Fermi level and actually cross it when an electric field is applied. Likewise, in the recent paper on the conducting properties of the $W_{18}O_{54}(SO_3)_2$ system, the eigenchannels correspond to combinations of W-4d orbitals.[31]

3.4 Adsorption properties of V18 on Au(111)

As stated in the introduction, the redox-chemistry of $[I@V_{18}O_{42}]^{5-}$ (V18) is much richer than the so-far discussed V6 species. In its resting state, the molecule has 10 unpaired electrons in the V-d band coupled to an overall singlet spin state. This leads formally to a V^{IV}:V^{V} ratio of 10:8, although a previous study has established that most vanadium centers have an average oxidation state somewhere between these two formal values.[26] This study also showed that V18 can directly be adsorbed on the gold surface without need for extra stabilizing capping ligands, although no information about the adsorption mode could be extracted from the experiment. Among the many possibilities, two adsorption modes has emerged as most stable ones from the present computational investigation. In both modes the V18 is attached to the gold surface by three O-Au contacts, two terminal oxygens bound to vanadium atoms of the outer ring and the third one is either a terminal oxygen bond to a vanadium of the inner ring (mode 1), or an apex vanadium (mode 2). As illustrated in Fig. 13, mode 1 attaches to the surface by an empty facet of the V18 molecule, while there is a three-fold bonded oxygen in mode 2. The distance of this μ_3-oxygen to the surface remains large and no direct interaction was observed with the surface.

Similar interaction energies were obtained for the four sites that we tested (see Fig. 13, right) with a slight preference for the top-top orientation, the top-hcp and hcp-bridge at 0.1 eV higher energy and the top-fcc was computed to have a 0.35 eV higher energy. A similar picture arises for mode 2, for which the top-top is 0.09 eV more favorable than in mode 1. The absolute interaction energy of the top-top in mode 2 is -1.2 eV, significantly larger than that obtained for V6 on Au(111). The three Au-O distances in mode 1 are 2.48 $\pm$0.02 Å. Mode 2 shows a larger spread in the distances (2.41, 2.47 and 2.51 Å), but they are on average also larger than those calculated for V6 on Au(111). This larger POV-Au distance is a direct consequence of the larger negative charge of the V18 molecule in comparison to the capped-V6 system. The larger polarizability of V18 is most probably the reason for the stronger interaction energy, despite the larger distance to the surface.

Bader charges and density difference plots indicate that the adsorption does not change the oxidation state of the V18 molecule. The calculated total charge of the V18 unit in adsorption mode 1 and 2 are -5.03 and -5.23, close to the 5- charge of the isolated molecule. The density difference plot shows larger areas of change than in the V6 case, in line with the larger polarizability. However, there is no clear sign of charge depletion or built-up on the molecule as the yellow and blue shaded areas are equally present on the molecule. The interpretation of the DOS (shown in Figure S4 in the supplementary information) is more complicated because of the presence of the partially filled V-3d band that cross the Fermi level, exactly the same energy region where also many Au levels appear. Due to the metallic character of the electrodes, the occupation of the levels near the Fermi energy has to be smeared out over a range of formally occupied and unoccupied bands. This partial occupation severely hinders the electron

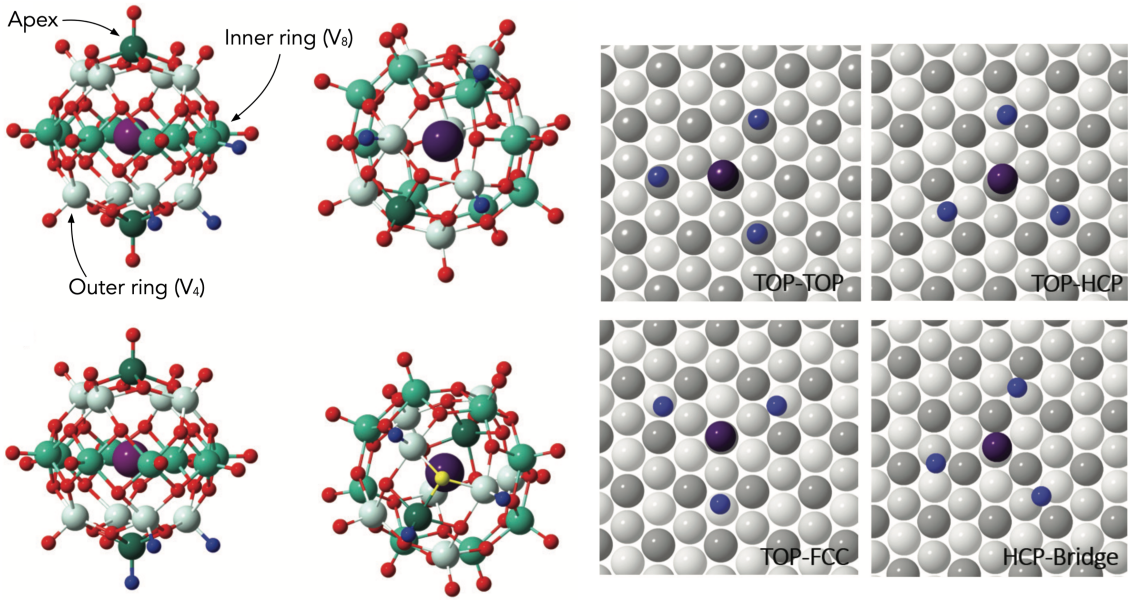

Fig. 13 Left: Au-O contacts in the two adsorption modes (top: mode 1; bottom: mode 2) of V18 on Au(111). Color code: green (dark, normal and light): vanadium; red: oxygen; purple: iodine; blue: oxygen attached to Au; yellow: μ_3-oxygen. Right: Schematic representation of the top-top, top-hcp, top-fcc and hcp-bridge adsorption positions for mode 1. Only the central iodine and the three O atoms attached to the surface are shown. The first label corresponds to the position of I with respect to the surface, the second indicates the position of the three O atoms.

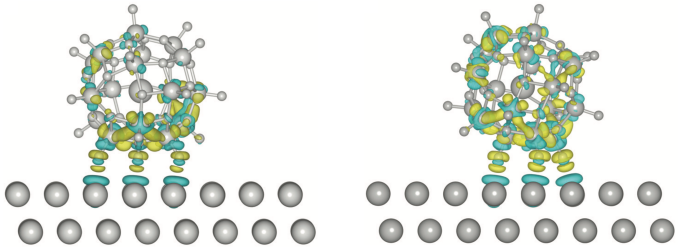

Fig. 14 Charge difference $\Delta\rho$ for the adsorption of V18 on Au(111) in mode 1 (left) and 2 (right). Yellow and blue regions represent accumulation and depletion of the electron density, respectively. The surface isovalue is set to 0.001 e/Bohr^{-3}.

count in the V-band; integration of the vanadium PDOS does not give access to the number of V-3d electrons as it does not take into account this smearing.

The Bader charges (see Table S2 in the supplementary information) steadily increase from -3.68 to -5.03 to -6.28 from the oxidized form V18(8:10) to the resting state V18(10:8) and to the reduced form V18(12:6). Polarization effects and countercation interactions prevent the observation of clean -2 changes between these three forms.

3.5 Transmission spectra of V18

Using the same electrode and tip model as in the V6 study, we have calculated the zero-bias transmission spectra of the three V18 forms to get a first idea of the possibility of observing staircase conductivity upon changes in the oxidation state. Figure 15 compares three calculated spectra in the -0.4···0.4 eV energy interval. Although far from identical, the transmission spectra of the three forms are qualitatively similar, showing a collection of high-, medium- and low-intensity peaks in the α channel in all cases. This behaviour is markedly different from the transmission spectra calculated for the V6 system herein analyzed. In the latter, we observed a steady increase of the number of peaks near the Fermi energy from one to two to three when comparing the fully oxidized form with the one-electron and two-electron reduced forms. The lack of such pronounced differences in V18 strongly suggests that the possibility of finding a staircase conductivity are rather slim for these oxidation states of the V18 molecule. The problem lies in the fact that the resting state has as many as 10 electrons in the V-3d band, which (as shown in Fig. S5 in the supplementary information) is the band with the largest contribution to the conduction channels. Hence, 8, 10 or 12 electrons do not constitute such an important change as going from 0 to 1 to 2 conduction electrons as in V6. A natural step to get a V6-like behaviour in V18 would be to reduce the number of valence 3d-vanadium electrons in the redox resting state. With this goal, one can envisage the ligand functionalization of the V18 surface as a possible strategy to vary its chemical nature and, thus, transform its redox properties.

4 Conclusions

The computational study of the molecular conductivity of polyoxovanadate molecules has shown that the experimentally observed staircase conductivity is intimately related to the changes in the conductivity of the molecules upon oxidation or reduction. The presence of extra electrons in the V-3d band increases the capacity of the molecule to transfer electrons from one electrode to the other. Reduction in itself does not lead automatically to staircase conductivity. The addition of one or two electrons must be accompanied by a significant change in the zero bias transmission spectrum, which only occurs for a relatively small number of elec-

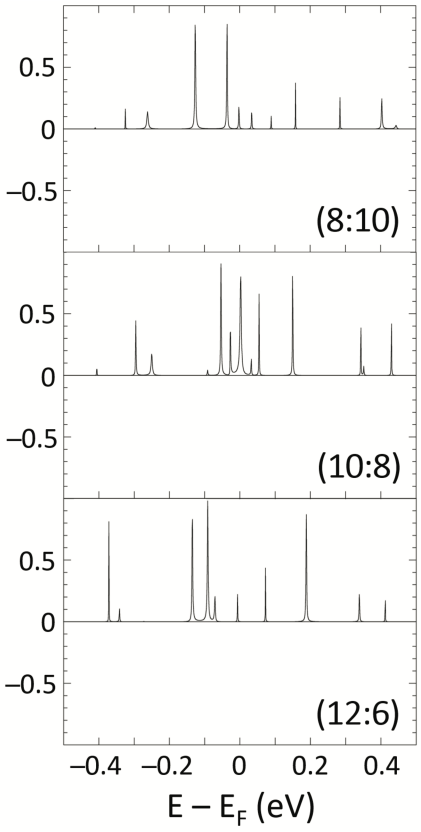

Fig. 15 Zero bias transmission spectra of V18(8:10), V18(10:8) and V18(12:6) in the vicinity of the Fermi energy.

trons.

In the two cases that were studied here, the capped-V6 adsorbed on Au(111) has zero electrons in the resting state, and hence, adding one, two or three electrons introduces qualitative changes in the transmission spectrum, leading to markedly different conductivity for the different oxidation states. On the contrary, V18 adsorbed on Au(111) has already ten electrons for conduction, and adding or subtracting two does not make enough of a difference to change the transmission significantly. In the search for new materials that can be used in memristive devices attention should be focused on those molecules that are easily reduced multiple times but do not have too many electrons in bands that are close to the Fermi level and expected to be responsible for the molecular conductivity.

Conflicts of interest

There are no conflicts to declare.

Acknowledgements

The authors thank Kirill Yu. Monakhov for fruitful discussions. Financial support has been provided by the Spanish Administration (CTQ2017-83566-P) and the Generalitat de Catalunya (2017-SGR629). The authors acknowledge the computer resources at MareNostrum and the technical support provided by Barcelona Supercomputing Center (QS-2019-3-0001 and QS-2020-1-0026).

References

1 M. T. Pope, *Heteropoly and isopoly Oxometalates*, Springer-Verlag, 1983.
2 M. T. Pope and A. Müller, *Angew. Chem. Int. Ed.*, 1991, **30**, 34–48.
3 L. Cronin, P. Kögerler and A. Müller, *J. Solid State Chem.*, 2000, **152**, 57–67.
4 A. Müller, P. Kögerler and H. Bögge, *Structure and Bonding*, 2000, **96**, 203–236.
5 D.-L. Long, R. Tsunashima and L. Cronin, *Angew. Chem. Int. Ed.*, 2010, **49**, 1736–1758.
6 A. V. Anyushin, A. Kondinski and T. N. Parac-Vogt, *Chem. Soc. Rev.*, 2020, **49**, 382–432.
7 J. Livage, *Coord. Chem. Rev.*, 1998, **178-180**, 999–1018.
8 Y. Hayashi, *Coord. Chem. Rev.*, 2011, **255**, 2270–2280.
9 A. Müller, R. Sessoli, E. Krickemeyer, H. Bögge, J. Meyer, D. Gatteschi, L. Pardi, J. Westphal, K. Hovemeier, M. Rohlfing, J. Döring, F. Hellweg, C. Beugholt and M. Schmidtmann, *Inorg. Chem.*, 1997, **36**, 5239–5250.
10 A. Kondinski and K. Y. Monakhov, *Chem. Eur. J.*, 2017, **23**, 7841–7852.
11 W. L. Queen, J. P. West, J. Hudson and S.-J. Hwu, *Inorg. Chem.*, 2011, **50**, 11064–11068.
12 J. M. Clemente-Juan, E. Coronado and A. Gaita-Ariño, *Chem. Soc. Rev.*, 2012, **41**, 7464–7478.
13 P. Day and E. Coronado, *Magnetism: Molecules to Materials V*, Wiley-VCH, 2005, ch. 4, pp. 105–159.
14 D. Gatteschi, R. Sessoli and F. Villain, *Molecular Nanomagnets*, Oxford University Press, Oxford, 2006.
15 M.-P. Santoni, G. La Ganga, V. Mollica Nardo, M. Natali, F. Puntoriero, F. Scandola and S. Campagna, *J. Am. Chem. Soc.*, 2014, **136**, 8189–8192.
16 M. L. Campbell, D. Sulejmanovic, J. B. Schiller, E. M. Turner, S.-J. Hwu and D. C. Whitehead, *Cat. Sci. Technol.*, 2016, **6**, 3208–3213.
17 S. Cardona-Serra, J. M. Clemente-Juan, E. Coronado, A. Gaita-Ariño, N. Suaud, O. Svoboda, R. Bastardis, N. Guihéry and J. J. Palacios, *Chem. Eur. J.*, 2015, **21**, 763–769.
18 K. Y. Monakhov, M. Moors and P. Kögerler, *Polyoxometalate Chemistry*, Academic Press, 2017, vol. 69, ch. 9, pp. 251–286.
19 X. Chen, Y. Zhou, V. A. L. Roy and S.-T. Han, *Adv. Mater.*, 2018, **30**, 1703950.
20 J. J. Yang, D. B. Strukov and D. R. Stewart, *Nature Nanotechnol.*, 2013, **8**, 13–24.
21 P. Sheridan and W. Lu, *Memristor Networks*, Springer, New York, 2014, pp. 129–149.
22 B. Dong, J. Peng, A. Tian, J. Sha, L. Li and H. Liu, *Electrochim. Acta*, 2007, **52**, 3804–3812.
23 T. D. Keene, D. M. D'Alessandro, K. W. Krämer, J. R. Price, D. J. Price, S. Decurtins and C. J. Kepert, *Inorg. Chem.*, 2012, **51**, 9192–9199.
24 H. Wan, C. Wang, Y. Zhang, H. Miao, S. Zhou and Y. Xu, *Inorg. Chem.*, 2014, **53**, 10498–10505.
25 K. Y. Monakhov, O. Linnenberg, P. Kozłowski, J. van Leusen,

C. Besson, T. Secker, A. Ellern, X. López, J. M. Poblet and P. Kögerler, *Chem. Eur. J.*, 2015, **21**, 2387–2397.
26 O. Linnenberg, M. Moors, A. Solé-Daura, X. López, C. Bäumer, E. Kentzinger, W. Pyckhout-Hintzen and K. Y. Monakhov, *J. Phys. Chem. C*, 2017, **121**, 10419–10429.
27 P. Kozłowski, A. Notario-Estévez, C. de Graaf, X. López and K. Y. Monakhov, *Phys. Chem. Chem. Phys.*, 2017, **19**, 29767–29771.
28 A. Notario-Estévez, P. Kozłowski, O. Linnenberg, C. de Graaf, X. López and K. Y. Monakhov, *Phys. Chem. Chem. Phys.*, 2018, **20**, 17847–17858.
29 A. Solé-Daura, A. Notario-Estévez, J. J. Carbó, J. M. Poblet, C. de Graaf, K. Y. Monakhov and X. López, *Inorg. Chem.*, 2019, **58**, 3881–3894.
30 O. Linnenberg, M. Moors, A. Notario-Estévez, X. López, C. de Graaf, S. Peter, C. Baeumer, R. Waser and K. Y. Monakhov, *J. Am. Chem. Soc.*, 2018, **140**, 16635–16640.
31 P. Lapham, L. Vilà-Nadal, L. Cronin and V. P. Georgiev, *J. Phys. Chem. C.*, 2021, **125**, in press.
32 O. Linnenberg, A. Kondinski and K. Y. Monakhov, *Supramolecular Systems: Chemistry, Types and Applications*, Nova Science Publishers, Hauppage, 2017, ch. 2, pp. 39–66.
33 X. López, J. A. Fernández and J. M. Poblet, *Dalton Trans.*, 2006, 1162–1167.
34 G. Kresse and J. Hafner, *Phys. Rev. B*, 1993, **47**, 558–561.
35 G. Kresse and J. Hafner, *Phys. Rev. B*, 1994, **49**, 14251–14269.
36 G. Kresse and J. Furthmüller, *Phys. Rev. B*, 1996, **54**, 11169–11186.
37 G. Kresse and J. Furthmüller, *Comput. Mater. Sci.*, 1996, **6**, 15–50.
38 X. Aparicio-Anglès, A. Clotet, C. Bo and J. M. Poblet, *Phys. Chem. Chem. Phys.*, 2011, **13**, 15143–15147.
39 X. Aparicio-Anglès, P. Miró, A. Clotet, C. Bo and J. M. Poblet, *Chem. Sci.*, 2012, **3**, 2020–2027.
40 Z. Lang, X. Aparicio-Anglès, I. A. Weinstock, A. Clotet and J. M. Poblet, *Inorg. Chem.*, 2017, **56**, 3961–3969.
41 J. P. Perdew, J. A. Chevary, S. H. Vosko, K. A. Jackson, M. R. Pederson, D. J. Singh and C. Fiolhais, *Phys. Rev. B*, 1992, **46**, 6671–6687.
42 P. E. Blöchl, *Phys. Rev. B*, 1994, **50**, 17953–17979.
43 J. Hafner, *J. Comput. Chem.*, 2008, **29**, 2044–2078.
44 S. Elliot, *Physics of Amorphous Materials*, Longman, Essex, U.K., 1990.
45 J. R. Hook and H. E. Hall, *Solid State Physics*, Wiley, New York, 2nd edn, 1995.
46 H. J. Monkhorst, *Phys. Rev. B*, 1976, **13**, 5188–5192.
47 J. D. Pack and H. J. Monkhorst, *Phys. Rev. B*, 1977, **16**, 1748–1749.
48 R. F. W. Bader, *Atoms in Molecules. A Quantum Theory*, Oxford University Press, Oxford, UK, 1990.
49 M. Yu and D. R. Trinkle, *J. Chem. Phys.*, 2011, **134**, 064111.
50 J. M. Soler, E. Artacho, J. D. Gale, A. García, J. Junquera, P. Ordejón and D. Sánchez-Portal, *J. Phys.: Condens. Matter*, 2002, **14**, 2745–2779.
51 N. Papior, N. Lorente, T. Frederiksen, A. García and M. Brandbyge, *Comp. Phys. Commun.*, 2017, **212**, 8–24.
52 N. Troullier and J. L. Martins, *Phys. Rev. B*, 1991, **43**, 1993–2006.
53 N. Troullier and J. L. Martins, *Phys. Rev. B*, 1991, **43**, 8861–8869.
54 M. Brandbyge, J.-L. Mozos and P. Ordejón, *Phys. Rev. B*, 2002, **65**, 165401.
55 C. Toher and S. Sanvito, *Phys. Rev. B*, 2008, **77**, 155402.
56 Z. Lang, *PhD thesis*, Universitat Rovira i Virgili, http://hdl.handle.net/20.500.11797/TDX2641, 2017.
57 S. Grimme, J. A. Antony, S. Ehrlich and H. Krieg, *J. Chem. Phys.*, 2010, **132**, 154104.
58 A. Bondi, *J. Phys. Chem.*, 1964, **68**, 441–451.
59 M. Mantina, A. C. Chamberlin, R. Valero, C. J. Cramer and D. G. Truhlar, *J. Phys. Chem. A*, 2009, **113**, 5806–5812.
60 N. Casañ-Pastor and L. C. W. Baker, *J. Am. Chem. Soc.*, 1992, **114**, 10384–10394.
61 N. Suaud, A. Gaita-Ariño, J. M. Clemente-Juan, J. Sánchez-Marín and E. Coronado, *J. Am. Chem. Soc.*, 2002, **124**, 15134–15140.
62 N. Suaud, X. López, N. Ben Amor, N. A. G. Bandeira, C. de Graaf and J. M. Poblet, *J. Chem. Theory Comput.*, 2015, **11**, 550–559.
63 C. de Graaf, R. Caballol, S. Romo and J. M. Poblet, *Theor. Chem. Acc.*, 2009, **123**, 3–10.
64 M. Paulsson and M. Brandbyge, *Phys. Rev. B*, 2007, **76**, 115117.
65 T. Frederiksen, M. Paulsson, M. Brandbyge and A.-P. Jauho, *Phys. Rev. B*, 2007, **75**, 205413.